Canalized gene expression during development mediates caste differentiation in ants

Bitao Qiu
Univerisity of Copenhagen https://orcid.org/0000-0003-4588-7680
Xueqin Dai
University of Chinese Academy of Sciences
Panyi Li
BGI–Shenzhen
Rasmus Larsen
University of Copenhagen
Ruyan Li
University of Copenhagen
Alivia Price
University of Copenhagen
Guo Ding
Kunming Institute of Zoology
Michael Texada
University of Copenhagen
Xiafang Zhang
Kunming Institute of Zoology
Dashuang Zuo
Kunming Institute of Zoology
Qionghua Gao
Guangxi University
Wei Jiang
BGI–Shenzhen
Tinggang Wen
BGI-Shenzhen
Luigi Pontieri
University of Copenhagen https://orcid.org/0000-0002-1506-3827
Chunxue Guo
China National Genebank, BGI-Shenzhen
Kim Rewitz
University of Copenhagen https://orcid.org/0000-0002-4409-9941
Qiye Li

BGI-Shenzhen https://orcid.org/0000-0002-5993-0312
Weiwei Liu
Kunming Institute of Zoology https://orcid.org/0000-0001-5082-9114
Jacobus Boomsma
University of Copenhagen https://orcid.org/0000-0002-3598-1609
Guojie Zhang (guojie.zhang@bio.ku.dk)
University of Copenhagen https://orcid.org/0000-0001-6860-1521

Article

Keywords:

Posted Date: March 16th, 2022

DOI: https://doi.org/10.21203/rs.3.rs-1432093/v1

Version of Record: A version of this preprint was published at Nature Ecology & Evolution on October 3rd, 2022. See the published version at https://doi.org/10.1038/s41559-022-01884-y.

Canalized gene expression during development mediates caste differentiation in ants

Authors:

Bitao Qiu[1,2,#,*], Xueqin Dai[3,4,#], Panyi Li[5], Rasmus Stenbak Larsen[1], Ruyan Li[1], Alivia Lee Price[1], Guo Ding[1,3], Michael James Texada[6], Xiafang Zhang[3], Dashuang Zuo[3], Qionghua Gao[3,7], Wei Jiang[5], Tinggang Wen[5], Luigi Pontieri[1], Chunxue Guo[5], Kim Rewitz[6], Qiye Li[5], Weiwei Liu[3], Jacobus J. Boomsma[2,*], Guojie Zhang[1,3,8,9,*]

Affiliations:

[1] Villum Center for Biodiversity Genomics, Section for Ecology and Evolution, Department of Biology, University of Copenhagen, Copenhagen, Denmark.
[2] Centre for Social Evolution, Section for Ecology and Evolution, Department of Biology, University of Copenhagen, Copenhagen, Denmark.
[3] State Key Laboratory of Genetic Resources and Evolution, Kunming Institute of Zoology, Chinese Academy of Sciences, Kunming, China.
[4] Kunming College of Life Science, University of Chinese Academy of Sciences, Kunming, China.
[5] China National GeneBank, BGI–Shenzhen, Shenzhen, China.
[6] Section for Cell and Neurobiology, Department of Biology, University of Copenhagen, Copenhagen, Denmark.
[7] Guangxi Key Laboratory of Agric-Environment and Agric-Products Safety, College of Agriculture, Guangxi University, Nanning, China.
[8] Center for Excellence in Animal Evolution and Genetics, Chinese Academy of Sciences, Kunming, China.
[9] Evolutionary and Organismal Biology Research Center, School of Medicine, Zhejiang University, Hangzhou, China
# These authors contributed equally.
* Corresponding authors: bitao.qiu.88@gmail.com (B.Q.); jjboomsma@bio.ku.dk (J.J.B.); guojiezhang@zju.edu.cn (G.Z.)

Abstract:

Ant colonies are higher-level organisms consisting of specialized reproductive and non-reproductive individuals that differentiate early in development, similar to germ-soma segregation in bilateral Metazoa. Analogous to diverging cell lines, developmental differentiation of individual ants has often been considered in epigenetic terms, but the sets of genes that determine caste phenotypes throughout larval and pupal development remain unknown. Here we reconstruct the individual developmental trajectories of two ant species after obtaining > 1400 whole-genome transcriptomes. Using a novel backward prediction algorithm, we show that caste phenotypes can be accurately predicted by genome-wide transcriptome profiling. We find that caste differentiation is increasingly canalized from early development onwards, particularly in germline individuals (gynes/queens), and that the juvenile hormone signalling pathway regulates this process with feedback from diverging larval body mass. We quantified gene-specific canalization levels and found that canalized genes with gyne/queen-biased expression were enriched for ovary and wing functions while canalized genes with worker-biased expression were enriched in brain and behavioural functions. Suppression in gyne larvae of *Freja*, a highly canalized gyne-biased ovary gene, disturbed pupal development by inducing non-adaptive intermediate phenotypes between gynes and workers. Our results indicate that the life cycle ontogeny of colonial superorganisms is maintained by strong purifying selection.

Introduction:

In his *Ants* monograph, William Morton Wheeler concluded that there is a striking analogy 'between the ant colony and the cell colony which constitutes the body of a Metazoan animal; and many of the laws that control the cellular origin, development, growth, reproduction and decay of the individual Metazoan, are seen to hold good also of the ant society regarded as an individual of a higher order' [1]. This century-old statement highlights putative parallels between (a) irreversible major transitions to organismal multicellularity with a differentiated germline and altruistic cellular soma, and (b) colonial superorganismality with physically differentiated queen and worker castes as higher-level germline and soma [2]. It implies that, once cell fate or caste fate have been determined early in development, individual cells or ant larvae should follow analogous developmental trajectories that give rise to terminally specialized cell types or morphologically distinct adult caste phenotypes, respectively.

Some decades later, Conrad H. Waddington depicted metazoan embryogenesis as a pebble rolling downhill in a rugged epigenetic landscape, with cells losing pluripotency as they commit to divergent valleys representing developmental trajectories [3,4]. In combination, these early insights suggest that there should be Waddington landscapes for ant colony development reflecting the analogous Wheelerian understanding of developmental processes at two different levels of organismality. While the molecular biology of differential gene expression has now largely replaced Waddington's organicist perception of development, his diagrams remain instructive heuristic tools for analogous understanding of genetic regulatory networks (GRNs) that affect cell differentiation in metazoan bodies and caste differentiation in ant colonies.

Recent advances in single-cell transcriptomics have revealed many molecular details of Waddington landscape differentiation [5–7] while reconstructing developmental trajectories in unprecedented detail and identifying key gene modules for cell fate determination [8]. However, no studies of comparable ambition have been pursued to track ontogenetic development of superorganismal colonies *sensu* Wheeler and quantify the canalization properties of caste differentiation. The phylogenetically diverse holometabolic ants, with their clear developmental stages, are particularly inviting to embark on such investigations, but studies have so far used pooled samples or obtained rather few individual transcriptomes [9–11], which has precluded formal analyses of individual heterogeneity during the entire developmental process of caste differentiation. In particular, whether the sequence of larval and pupal caste differentiation is a canalized developmental process, in which specific genes initiate and regulate cascades of differential gene expression while shaping morphologically diverging phenotypes, is unknown.

We used low-input RNA-sequencing to obtain more than 1400 genome-wide individual transcriptomes covering the major developmental stages of *Monomorium pharaonis* and *Acromyrmex echinatior*, while using *Drosophila melanogaster* for outgroup comparisons. These two ant species belong to the same subfamily, Myrmicinae, but differ in social and developmental characteristics. *M. pharaonis* is a highly polygynous (multi-queen) invasive

ant, while *A. echinatior* is a fungus-growing leaf-cutting ant with mostly single queen colonies but, in contrast to *M. pharaonis*, a polymorphic worker caste with small nursing workers and large workers for foraging and colony defence [12,13]. We reconstructed developmental trajectories for gyne and worker caste differentiation via genome-wide gene expression profiling, using a novel algorithm for predicting caste phenotype before larvae express morphological differences. We then focused on the larval-pupal transition to quantify caste-specific canalization effects and their underlying pathways, and finally examined some of the key genes regulating the canalization of caste phenotypes.

Results:

A transcriptomic atlas for ant development

Developmental trajectory networks constructed from whole-genome transcriptomes (Fig. 1a and Extended Data Fig. 1a; Methods) clustered individuals primarily by developmental stage and gradually also by caste phenotype. Adjacent developmental stages always grouped next to each other, as expected when development is a largely continuous process, but we also observed distinct clusters in early embryonic stages (0 – 24 h) and for the late larvae to early pupae transition, indicating more discrete stage-specific transcriptomes. Principal Component Analysis (PCA) for both species showed a first axis separating the two ant species while the second and third axes jointly separated individuals by developmental stage and caste identity (Fig. 1b).

Aligning developmental transcriptomes showed 67-81% similarity between the two ant species across the developmental stages (Fig. 1c), reflecting considerable conservation of developmental gene regulatory networks (GRNs) in the Myrmicinae subfamily to which both ant species belong. Developmental transcriptomes were more similar for gynes than for workers across the developmental stages, both when comparing the two ant species with each other, and when contrasting the two *M. pharaonis* caste profiles with those of *D. melanogaster* females (Fig. 1c). These patterns are consistent with gyne development being under stronger selection constraint than worker development across social insects with permanent caste differentiation [11]. However, it is important to acknowledge that gynes are elaborations of the ancestral reproductive phenotype of solitary female Hymenoptera, while differentiated worker castes are later innovations whose foundational GRNs evolved analogously, not homologously, in superorganismal ants and bees [14].

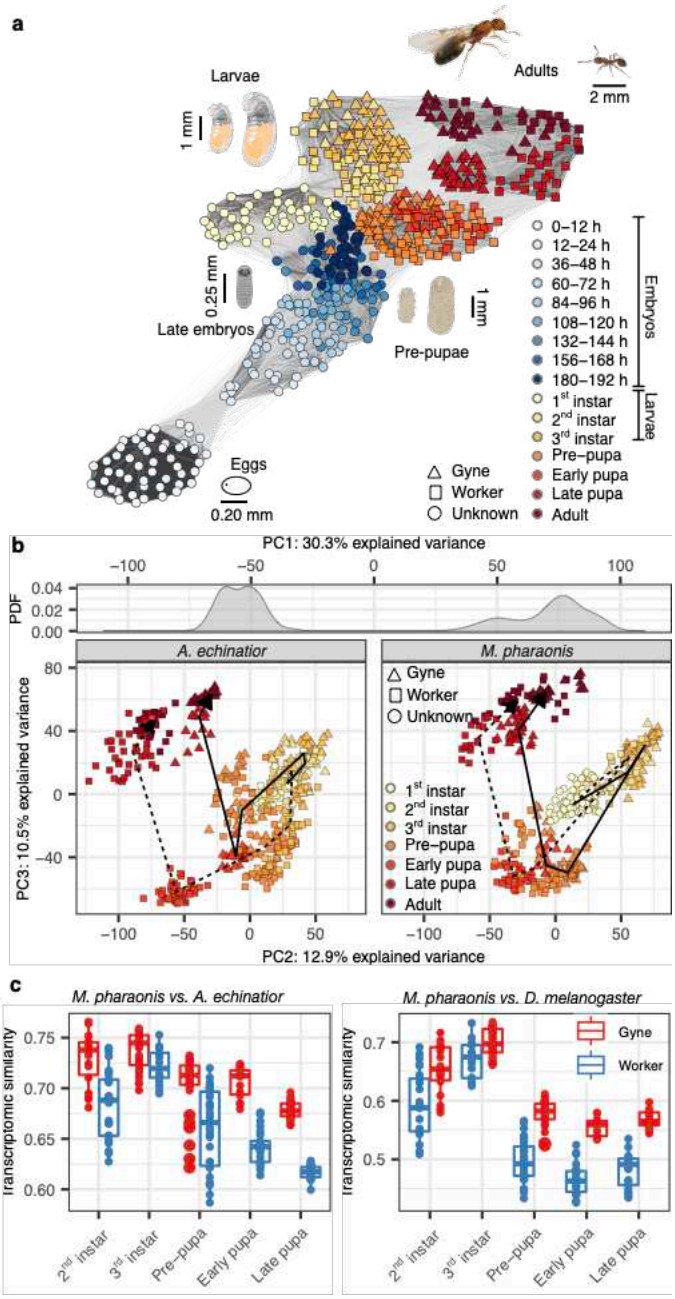

Fig. 1. Homologous caste differentiation trajectories in two ant species.
a, *M. pharaonis* developmental trajectories reconstructed from 568 individual transcriptomes covering all developmental stages. Shading of connecting lines reflects the strength of mutual transcriptome correlations, ranging from 0.8 (light grey) to 1.0 (black). Symbol colours differentiate between embryos within eggs (white and blue), larvae (yellow), pupae (red), and adults (brown). Image courtesies: Anna Mosegaard Schmidt (adult gyne) and Luigi Pontieri (worker).
b, The first three PC axes for individual transcriptomes of *A. echinatior* and *M. pharaonis*, from 1st instar larvae to adults. Upper panel: probability density function (PDF) of PC1 values separating the two ant species; Lower panel: PC2 and PC3 jointly distinguish between developmental stages and caste phenotypes across individual transcriptomes. Lines connect the median PC values for each caste across development stages, showing that individuals follow very similar trajectories regardless of species identity. Symbol colours and shapes as in the a-panel.
c, Between-species transcriptome similarities comparing *M. pharaonis* and *A. echinatior* (left) and *M. pharaonis* and *D. melanogaster* females (right), based on stage-specific Spearman correlation coefficients and plotted separately for gynes (red) and workers (blue). Between-species similarities

peaked in 3rd instar larvae where gynes and workers were similar, but were always lower in earlier and later stages where worker similarities were also lower than gyne similarities.

Predicting caste phenotypes in small, morphologically undifferentiated larvae

Morphological differences between gyne and worker individuals cannot be detected before the 2nd and 3rd larval instar in *M. pharaonis* and *A. echinatior*, respectively [12,15]. To identify individual caste phenotypes in earlier stages lacking morphological markers, we developed the *Backward Progressives Algorithm (BPA)* that retrospectively infers the likelihood of individuals belonging to one caste or another (Methods; Extended Data Fig. 2a). BPA assumes that key genes active in the GRN at a specific stage should, albeit with modified expression, also participate in caste differentiation during the subsequent developmental stage, analogous to what is known for key transcription factors that specify cell types during metazoan development [5,8,16]. We validated BPA using embryonic sex differentiation data from *Drosophila* (Extended Data Fig. 2b) and confirmed the accuracy of BPA in samples of *M. pharaonis* larvae with known caste identity (Extended Data Fig. 2c).

We applied BPA to 54 transcriptomes of 1st instar *M. pharaonis* larvae (Fig. 2a) and predicted 12 of these to be reproductives (gynes and males) and 18 to be workers with > 90% probability. We validated these predictions with RNA fluorescent *in situ* hybridization (HCR-FISH [17]) to assess the expression co-localization between *vasa*, a germ-line marker of 1st instar larvae and late embryos [18] (Extended Data Fig. 2d), and *LOC105839887* and *histone-lysine N-methyltransferase SMYD3* (*LOC105830671*). These two genes exhibit strong differential expression between predicted 1st instar caste phenotypes (Supplementary table 1) and have binary gyne-worker expression in 2nd instar larvae. First instar *LOC105839887* expression is visible in fat-bodies while *SMYD3* co-localizes with *vasa* in the larval gonads (Fig. 2b, left panel). Both genes could be unambiguously detected in individuals with a *vasa*-specified germline and were always absent in individuals without a germline (Fig. 2b, right panel).

We also applied BPA in *A. echinatior* where we lacked morphological markers for 2nd and 1st instar larvae. While third instar gyne larvae of this species can be unambiguously distinguished from worker larvae by their full-body curly hairs [12], this pilosity is not yet expressed in 2nd instar larvae. BPA found that the first two PC axes constructed from the 2nd instar transcriptomes separated 2nd instar larvae by body size and 3rd instar larvae by caste identities (Fig. 2c). Further inspection showed that the larger 2nd instar larvae (suspected gynes) in fact have some gyne-like curly hairs in their ventral thorax region (Extended Data Fig. 2e), indicating that caste differentiation in *A. echinatior* begins before the 2nd larval instar. To our knowledge, BPA is the first algorithm to achieve such accurate backwards predictions of developmental stages.

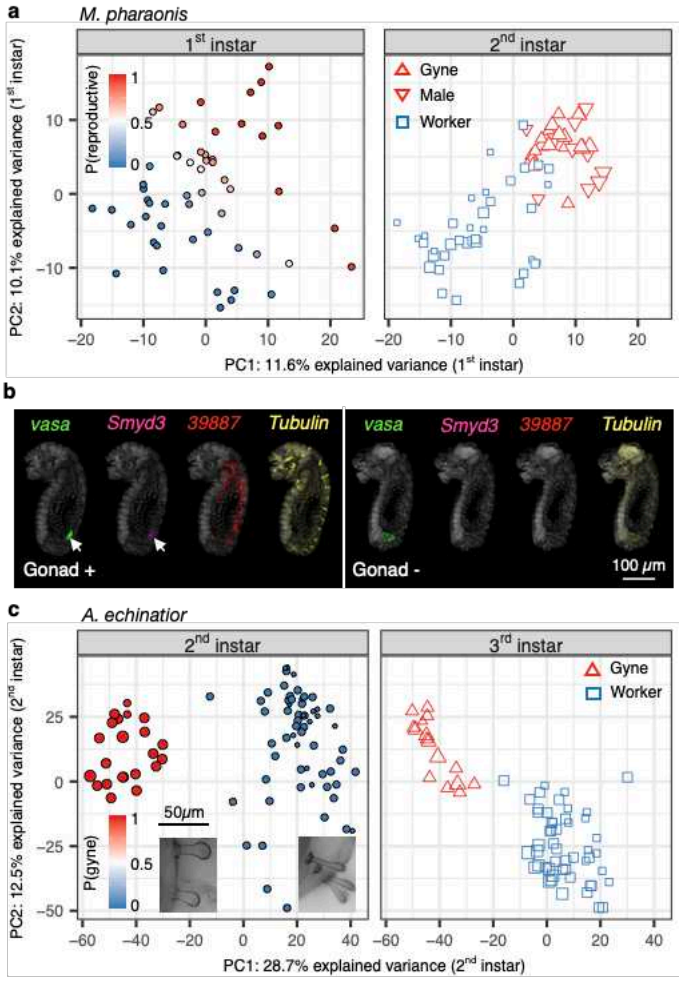

Fig. 2. BPA predicts individual caste phenotypes independent of external morphological traits.
a, BPA predictions of early caste identity in *M. pharaonis*, showing that the first two PC projections from 1st instar larvae (*n* = 54) match reproductives (an unknown mix of gynes and males) and workers among 2nd instar larvae (*n* = 66). Colours of 1st instar sample symbols reflect the predicted probability to be a reproductive individual (left panel) and identify individuals with morphologically validated caste and sex in 2nd instar larvae while also visualizing body length (right panel).
b, HCR-FISH staining for two of the best predictor genes of caste in 1st instar *M. pharaonis* larvae based on presence (+) or absence (-) of gonad tissue, i.e. *LOC105839887* (red; expressed in fat bodies) and *Smyd3* (purple; expressed in gonads, white arrow), indicating that transcriptome-wide BPA assignments as gynes were correct because these two genes can only be detected in individuals with a germline (left Gonad+ panel). Germline presence was independently checked by *vasa* expression (green), showing that these transcripts were always undetectable in individuals without a germline (right Gonad- panel). The housekeeping gene *Tubulin* (yellow) was stained as a positive control (right images in both panels).
c, BPA predictions of early caste identity in *A. echinatior* larvae, showing that the first two PC projections from 2nd instar larvae (*n* = 84) matched the 3rd instar individuals (*n* = 67) with known caste morphology. Individual samples are coloured according to their predicted probability of being gyne or worker in the 2nd instar (left panel) while visualizing individual body lengths via the symbol diameters. Known gynes and workers in the 3rd instar are represented by triangles and squares (right panel) confirming BPA segregation. The inserted epifluorescence microscope hair images refer to the ventral thorax region of a typical predicted 2nd instar gyne (left) or worker (right).

Caste differentiation in ants is developmentally canalized

We next focused on the overall degree of canalization in genome-wide gene expression, defined as the statistical tendency for individual transcriptomes to start with a unimodal (pluripotent) distribution and gradually change to a bimodal (phenotypically committed) distribution with increasingly distinct peaks as development proceeds. We first quantified the distributions of genome-wide developmental potential (Δ) as a gyne or worker individual, using deviations in gene expression from average target profiles in subsequent developmental stages (Methods). Δ-values range between -1 and 1, with a positive value representing gyne-biased development and a negative value worker-biased development. We found that the absolute Δ-value between castes increased steadily in both ant species, while the variance of Δ-values within castes becomes gradually reduced as development proceeds (Fig. 3a and Extended Data Fig. 3). During this process, transcriptomic canalization in gynes was invariably stronger than in workers, both in transcriptomic variation *per se*, and in PCA patterns (Extended Data Fig. 3).

JH signalling regulates developmental caste canalization

Genome-wide transcriptomic canalization amplified beyond the 3rd instar when pupal metamorphosis starts (Fig 3a), a critical stage in all holometabolous insects [19]. To understand the entirety of upstream regulation of caste differentiation, we used generalized linear models to account for the effect of larval body mass (Methods) [20] and identified 65 conserved genes with parallel gyne-worker bias that were associated with larval differentiation in both ant species (Supplementary Table 2). These early caste DEGs are significantly enriched for genes involved in fatty acid and hormone metabolism (Supplementary Table 3) - orthologs of these genes with gyne-biased expression are also highly expressed in the fat-body tissues and tracheal system of *Drosophila* larvae (Extended Data Fig. 4a). In addition, multiple larval caste DEGs are associated with the juvenile hormone (JH) pathway, a key regulator of larval growth and molting in insects [19,21]. These included the genes *daywake*, encoding a haemolymph JH-binding protein, *LOC118646735*, a duplicate gene of *Drosophila juvenile hormone acid O-methyltransferase (jhamt)*, and *hexamerin* [22] (Extended Data Fig. 4b), confirming the important role of JH for caste differentiation [23,24].

We found that many genes involved in JH and ecdysone metabolism exhibited both body-length and caste-specific expression when larvae transition from the 3rd instar to the prepupal stage (Fig. 3b and Extended data Fig. 5a). In particular, the expression of *jhamt*, which delays the metamorphic molt[25], decreased in 3rd instar worker larvae when body length exceeded 0.7 mm, while expression in gyne larvae did not decrease until larvae had reached twice that length of 1.4 mm (Methods) (Fig. 3b). A similar difference occurred in the expression of *Ecdysone-induced protein 93 (E93)*, a downstream transcription factor of the JH pathway for initiating metamorphosis [26] (Fig. 3b), which increased when worker larval body length exceeded 1.4 mm but not in gyne larvae before they had reached 2.0 mm.

To experimentally prove the role of JH in caste canalization, we fed a JH analog (JHA) to 3rd instar worker larvae and a JH inhibitor, [27], to 3rd instar gyne larvae of *M. pharaonis* and found

that JHA significantly increased worker body length and precocene-I significantly reduced gyne body length (Fig. 3c). Furthermore, wing-buds and simple eyes (ocelli), both typical gyne characters, were induced in the JHA fed worker larvae (Extended Data Fig. 5c) while precocene-I treated gyne larvae had a significantly higher frequency of abnormal wings when they hatched as adults ($P < 0.05$ for Fisher's exact test; Extended Data Fig. 5d). These aberrant development results confirm that the JH signalling pathway is a key regulator for caste canalization in ants.

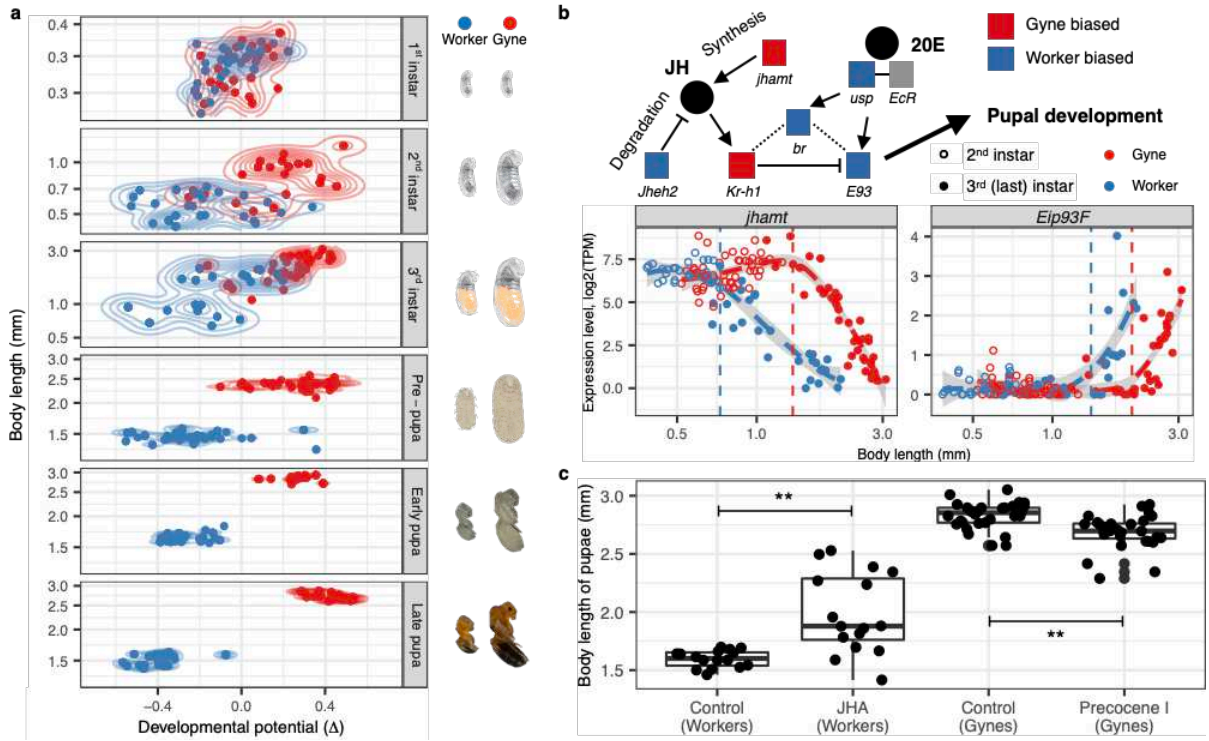

Fig. 3. Individual transcriptomes quantify caste canalization and its regulation by the JH signalling pathway.

a, Developmental potential scores (-1<Δ<1) reflecting caste commitment for gyne (positive) and worker (negative) phenotypes across developmental stages of *M. pharaonis* as body length increases, corresponding to the representative images towards the right (courtesy: Luigi Pontieri).

b, Caste- and body-length-specific expression of Juvenile Hormone (JH) and ecdysone (20E) pathways, coloured according to gyne-biased (red) or worker-biased (blue) expression in 3rd instar larvae (upper panel). The expression of *Juvenile hormone acid O-methyltransferase* (*jhamt*) and *Ecdysone-induced protein 93* (*E93*) showed both caste-specific (qualitative) and body-size-specific (quantitative) thresholds (vertical dashed lines; estimated with a threshold regression model [28] (Methods)) (lower panel). Note that the downregulation of *jhamt* (terminating the JH biosynthesis) preceded the upregulation of *E93* to actively initiate metamorphosis (see Extended Data Fig. 5a for expression patterns of other genes in this pathway).

c, In 3rd instar larvae of intermediate body length, feeding with JH analog (JHA) increased worker pupal body length (two-sided *t*-test; $P = 0.0004$; d.f. = 16.38; $t = 4.44$; $n = 16$ for both control and treatment groups), while precocene-I decreased gyne pupal body length (two-sided *t*-test; $P = 0.0001$; d.f. = 50.70; $t = -4.13$; $n = 30$ and 28 for control and treatment group, respectively).

Focal genes mediating canalization

To understand which genes are actually canalized during caste differentiation in the pupal stage, we developed a gene-specific *canalization score* (*C*) to track the developmental dynamics of between-caste gene expression divergence via the ratio of between-caste gene expression difference and stage-specific expression variance within castes (Methods). We identified 1140 and 2478 genes showing canalized expression in *M. pharaonis* (gynes *versus* workers) and *A. echinatior* (gynes *versus* small workers), respectively (C score > 3 and $P <$ 0.05 in one-sided Spearman's correlation tests) (Fig. 4a and Supplementary table 4). Among these canalized genes, 457 showed the same caste-bias direction in both species, a significantly higher number than the background expectation of 88 ($P < 10^{-15}$; Fisher's exact test), indicating that gene-level canalization is evolutionarily conserved. Thus, the number of differentially canalized genes in the pupal stage is seven time higher than the 65 genes in 3rd instar larvae, the last larval stage before the onset of pupation.

Comparison of the conserved canalized genes with tissue-level gene expression data in *Drosophila* [29] showed that gyne-biased canalized genes were highly expressed in ovaries, whereas worker-biased canalized genes were highly expressed in the brain and central nervous system (Extended Data Fig. 6a). Further analyses indicated that gyne-biased canalized genes were significantly enriched in flight muscle functions (e.g., *tropomyosin-2* (*Tm2*), *troponin I* (*TnI*) and *troponin C* (*TnC*)) and female reproductive functions (e.g., *T-complex protein 1* (*Tcp-1*), *krasavietz (kra)* and *merry-go-round* (*mgr*)) ($P < 0.05$ for both categories in hypergeometric tests). In contrast, worker-biased canalized genes were significantly enriched in neuronal and behavioural processes ($P < 0.05$ for both categories in hypergeometric tests), including *twin of eyeless* (*toy*), *hormone receptor 51* (*Hr51*) and octopamine receptors (*Octbeta1R* and *Octalpha2R*). These gene functions in a solitary insect are consistent with gyne caste specialization being targeted at dispersal and reproduction and worker caste specialization at more variable 'somatic' social tasks (Fig. 4a; Extended Data Fig. 6b; Supplementary table 5).

***Freja* as master regulator of queen phenotype**

The top gene with gyne-biased canalization in *M. pharaonis* is Hymenoptera-specific (Methods) and encodes a protein containing a predicted signal peptide and a leucine-rich-repeat domain (Extended Data Fig. 7a). Caste-biased expression of this gene begins in 2nd instar larvae and amplifies as development progresses (Extended Data Fig. 7b). In adult gynes, this gene is mainly expressed in the ovaries (Extended Data Fig. 7c) where its expression is restricted mostly to the ovarian follicle cells (Fig. 4b) which are essential for oogenesis [30]. We therefore named this gene *follicle related [gene-]expression in juvenile ants* (*Freja*, goddess of fertility in Old Norse).

We investigated *Freja*'s function through RNAi knock-down in late 3rd instar gyne larvae. Relative to *GFP*-RNAi controls, adults of the *Freja*-RNAi treatment group had significantly reduced body and head size (two-sided *t*-tests; $P < 10^{-4}$ for both; Fig. 4c) and a higher frequency of abnormal wing morphology. As wings and large bodies relative to workers are

unambiguous phenotypic markers of the adult reproductive (gyne/queen) caste in ants, we conclude that manipulation of *Freja* expression disturbed normal developmental canalization.

Because *Freja* remains highly expressed after pupal eclosion, we also manipulated *Freja* expression in adult *Monomorium* gynes with RNAi and examined effects on fertility. Both the size and the number of oocytes were significantly reduced in the *Freja*-RNAi group compared to the controls (two-sided *t*-tests; $P < 0.05$ for both; Fig. 4d and Extended Data Fig. 7e), indicating that *Freja*'s continued expression is crucial for gyne maturation and fertility after insemination. Thus, in addition to its necessary role in canalization of larval caste divergence, *Freja* maintains its differentiating functionality in adult gyne phenotypes. However, *Freja* was not a canalized gene in *A. echinatior*, a species where workers have retained ovaries to produce unfertilized (male) or inviable trophic eggs [31] (Extended Data Fig. 6).

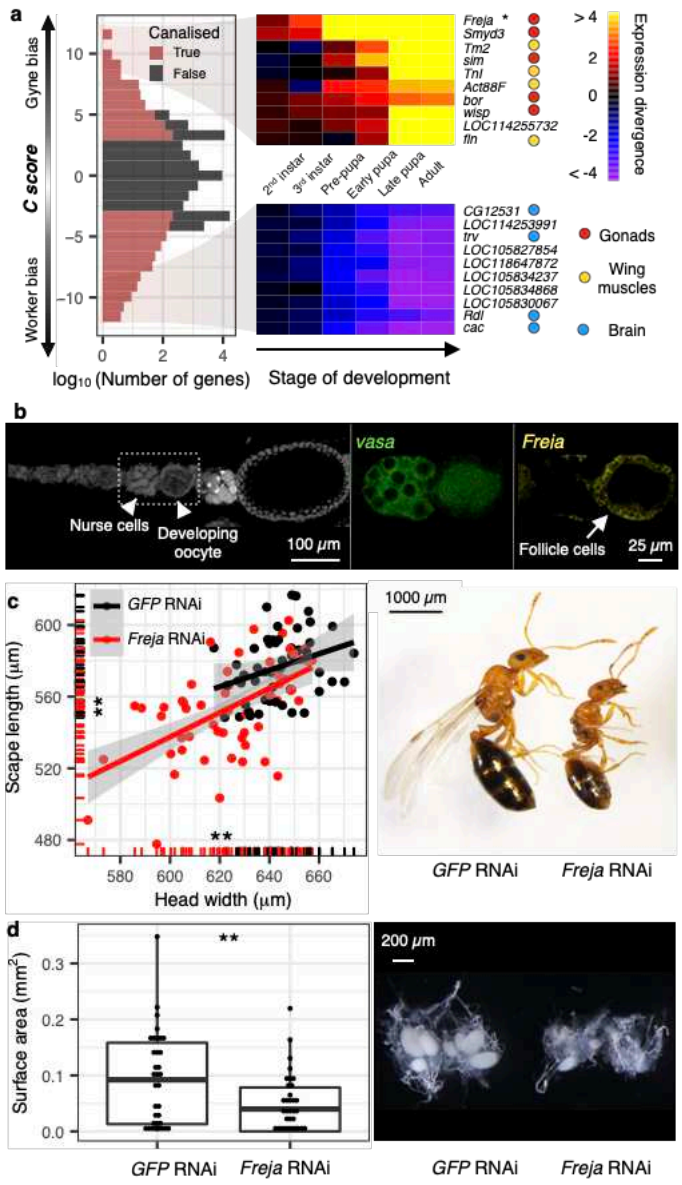

Fig 4. *Freja* and other major caste canalizing genes in *M. pharaonis*.
a, Overall gene-specific canalization scores (left) with the ten most strongly gyne-biased (top center) and worker-biased canalized genes (bottom center) visualised in heatmaps and colour coded by their tissue-expression in *D. melanogaster* (right).
b, HCR-FISH staining of *vasa* (middle, green) and the top canalized gene, *Freja* (right, yellow) in an adult gyne ovariole (left), showing *Freja* expression in ovarian follicle cells.
c, Compared to *GFP*-RNAi controls (black, n = 51), *Freja*-RNAi-treated 3rd instar gyne larvae (red, n = 58) produced pupae with reduced antennal scape length and head width (two-sided t-tests; d.f. = 102.47 and 93.63, and t = -5.43 and -5.61, respectively; both $P < 10^{-6}$; left) and more frequent abnormal wing development or complete lack of wings (16/66, 24.2%) compared to the control group (4/55, 7.3%) (P = 0.01; two-sided Fisher exact test; right).
d, Compared to *GFP*-RNAi controls (n = 34), *Freja*-RNAi-treated adult gynes (n = 33) induced lower mass and number of oocytes (two-sided t-tests; d.f. = 55.31 and 57.51, t = -2.40 and -3.03, and P = 0.02 and 0.004, respectively; see also Extended Data Fig. 7e), impairing overall reproductive functionality.

Discussion:

We have shown that ant caste differentiation is canalized throughout development in a way that is remarkably analogous to the canalized development of metazoan cell lineages starting with the first cell divisions of a zygote, a functional similarity that was noted more than a century ago [32]. Also the deeper conservation of colony-level germline development appears broadly convergent to what is known from animal development [6,33]. This suggests that ant colony-level ontogeny, unfolding as caste differentiation, has been maintained by strong stabilizing selection, in spite of substantial modifications in the details of caste differentiation during the huge adaptive radiation of the ants. The JH signalling pathway, known to be important for caste differentiation in social insects [23,34–37], appears to play a crucial role in regulating much of the canalization process of caste phenotypes via the control of, and feedback by, individual body size in the larval stages.

Our study is the first to have used an algorithmic approach (BPA) to predict caste phenotypes backwards in developmental time to identify gene markers before morphological caste differences emerge, a technique that should be broadly applicable in other kinds of developmental differentiation studies. Our analyses strongly suggest that caste is determined by the interaction of body size and gene expression, rather than by one of these factors alone [38]. We covered the entire developmental process, starting with genome-wide transcriptomics and then zooming in on the JH and ecdysone pathways to finally focus on specific genes with key roles in canalization of caste development. Intriguingly, experimental inhibition of *Freja* finally showed that disruption of canalized genes results in non-adaptive intermediate phenotypes between gynes and workers, both early in development and in adults.

Our findings emphasize that superorganismal colonies are shaped by higher-level adaptations to predictably reproduce entire life-cycles. In this process, the complementary development of caste phenotypes requires coordination and buffering via expression changes of canalized genes, analogous to the dynamic expression regulation of cell lineages during development of organismal metazoan bodies [5,39,40]. At the same time, our results indicate that even canalized developmental pathways can be changed when variation emerges and selection for directional change in caste phenotype is strong enough.

Methods:

Experimental design

We performed ultra-low-input transcriptome sequencing for individual samples of two ant species, *Monomorium pharaonis* and *Acromyrmex echinatior* (both subfamily Myrmicinae), covering four larval stages, the pre-pupal stage, the early and late pupal stage, and the adult stage (Extended Data Table 1). We also obtained individual transcriptomes for nine embryonic stages (starting 12 hours after egg laying and continuing sampling of older eggs with 12-hour intervals) in *M. pharaonis*. In this ant species, caste is known to be determined 'blastogenically' in early embryos [41,42], unlike most other ants where caste phenotype is determined during larval development [43]. For later developmental stages where caste phenotypes were morphologically distinguishable (Extended Data Table 2), we collected ca. 30 individuals per caste (gynes and workers in *M. pharaonis*; gynes, large workers and small workers in *A. echinatior*) for each stage (Extended Data Table 1). For stages where caste phenotype could not be identified morphologically (before the 2nd instar in *M. pharaonis* and before the 3rd instar in *A. echinatior*), we collected 30 eggs or 60 larvae per stage in order to transcriptomically infer caste. We also measured body length and head capsule width for all larval individuals to obtain another measure of developmental age that we integrated with transcriptomic information during analyses. We further obtained reference individual transcriptomes for *Drosophila melanogaster*, covering development from newly laid eggs to newly eclosed adults, sampling ca. 20 eggs at 3-hour intervals and ca. 20 larvae at 6-hour intervals. To ensure that individuals remained technically comparable, we processed samples of the same stages with the same experimental procedure and added ERCC spike-in RNA so we could check sample quality (RNA concentration) before sequencing [44]. We generated ca. 8 Gb RNA-seq data for each individual sample with paired-end ultra-low input RNAseq on BGIseq-500 platforms. After removing 63 samples of poor quality (RIN < 4 or having within-stage Spearman correlation coefficients with other transcriptomes < 0.8), we retained 819, 629 and 481 individual samples for *M. pharaonis*, *A. echinatior* and *D. melanogaster*, respectively.

Sample collection

M. pharaonis

Two colonies (D03 and 4030) of *M. pharaonis* were used in this study. Both were derived from interbreeding a global variety of genetic lineages and have been kept in captivity at the University of Copenhagen since 2004 [13], so they had substantial genetic variation in spite of having been propagated as pure lines since collection. Colonies were kept at 27 °C and 50 % relative humidity throughout the experiment. Individual samples were collected between January 2017 and March 2018. Because production of sexuals only occurs in colonies without queens (Q-) [45], we set up Q- sub-colonies from which all larvae, pupae and adults were collected. Collections of 1st-instar larvae were made more than 8 days after queens had been removed to ensure these larvae would include sexual-destined individuals following the insights obtained earlier [45,46].

To collect samples of developing embryos, we set up sub-colonies by isolating approximate 10 queens and 100 workers. Queens were left to lay egg for 12 hours (an average queen produces ca. 1-2 eggs per hour) [47], after which the queens were removed. We then collected at least 20 eggs at nine time points throughout embryo development: 0-12, 12-24, 36-48, 60-72, 84-96, 108-120, 132-144, 156-168 and 180-192 hours after oviposition (egg laying). At 192 hours after oviposition, embryos are in the last stages of embryo development (stage 14 to 17), so we were sure to have covered the entire egg stage of embryonic development. To minimize disturbance, a series of sub-colonies for embryo collection were setup independently for each developmental time point, so each sub-colony was only used once.

Individuals sampled as egg, larva, pupa or callow (adult/imago just after eclosion) were carefully collected, photographed (except eggs) (Leica MZ125 microscope) and stored individually, before being flash frozen in liquid nitrogen and stored at -80 °C until extraction.

A. echinatior

Three colonies of *A. echinatior* were used for this experiment, all collected in Gamboa, Panama (Ae150 collected on 19-04-2001, Ae394 collected on 28-04-2009 and Ae506 collected on 10-05-2011). Colonies were kept at 25 °C and 70 % relative humidity and were fed bramble leaves, rice and apples tree time a week. Individual samples were collected between March 2016 and November 2018. Larvae, pupae and callows were carefully removed from the fungus garden and individually photographed (Canon EOS 7D MarkII with macro lens EF 100mm). Samples were stored as in *M. pharaonis*.

D. melanogaster

We used the inbred wild-type genetic background *Canton-S* of *Drosophila melanogaster* for the experiment. Fly cultures were kept at 25 °C and 60% relative humidity throughout the experiment, with a 12-hour/12-hour light/dark cycle on standard *Drosophila* medium (commercial NutriFly medium, “Bloomington” recipe; Gennessee Scientific). Individual samples were collected between July 2017 and April 2018. Prior to egg collections the adult flies were purged of retained eggs by incubating in egg-laying chambers overnight with apple-juice/agar dishes covered with yeast paste. Eggs for experimental use were collected by swapping with a new freshly yeasted dish and incubating for 2 hours. Embryos were left on these plates for 24 hours until hatching, after which larvae were manually transferred with a fine probe to culture tubes of standard medium. Flies of the selected life stages were individually removed from culture media, rinsed in deionized water. Samples were stored as in *M. pharaonis*.

Identifying developmental age and separating worker, gynes and males

For both ant species, individual samples of larvae and pupae were laterally photographed during collection, after which body length and head capsule width (only for larvae) were measured using Adobe Photoshop CC 19.1.6 or ImageJ 1.53c. To distinguish males and females, we extracted DNA from each individual sample during the RNA extraction process

(see *RNA and DNA extraction for individual samples*). We identified the developmental age and separating different castes and sexes with the following procedures:

M. pharaonis

Developmental stages of *M. pharaonis* were estimated based on their body length and morphological characters (see Extended Data Table 2) [15,45]. Developmental stages of early and late pupae were determined by visual assessment of cuticle colour (males turn black and females turn brown), using a colour scale obtained from age-controlled pupae. Pupal deployment takes 12 days at 27 °C, so we selected early pupae between 0-2 days and late pupae between 10-12 days after the onset of pupation. Callow adult ants were collected based on their light cuticle colour, corresponding to ages a few days after eclosion.

From the 2nd-instar larval onwards, workers and sexuals (males and gynes) can be distinguished by morphological traits (see Extended Data Table 2). To further distinguish males and gynes (females) among the 2nd and 3rd-instar larval and pre-pupal sexuals, we used microsatellite genotyping (on the extracted DNA) to identify whether an individual was a haploid (male) or diploid (female), using five highly polymorphic nuclear microsatellite loci, with primer set: Mp4, Mp8, Mph2, Mph23 and Mph9 [13]. Repeat lengths of microsatellite loci were determined on an Applied Biosystems, Hitachi 3130xl, Genetic Analyzer and analysed using GeneMapper 4.0 software (Applied Biosystems).

A. echinatior

Developmental stages of larvae were estimated based on their body length and morphological characters (see Extended Data Table 2) [12], also see: https://megalomyrmex.osu.edu/temp/acro-larva-key/). The ages of pupae and callow adults were estimated by visual assessment of cuticle colour. Pupal development lasts between 20 – 27 days (own lab observations; see also [48]), so our samples of early and late pupae refer to the beginning and end of this range. Castes and sexes of 3rd and 4th-instar larvae and pre-pupae were distinguished based on the hair morphology (see Extended Data Table 2). To further distinguish males and females among 1st and 2nd-instar larvae where morphological markers for caste identity are not available, we used microsatellite genotyping to identify whether an individual was haploid (male) of diploid (female), using four highly polymorphic nuclear microsatellite loci (primer set: Acrin02, Acrin05, Acrin22, Acrin29 [12]. Repeat lengths of microsatellite loci were determined as in *M. pharaonis*.

D. melanogaster

For *D. melanogaster* we use chronological age to collect selected developmental stages (Extended Data Table 1). We used genotyping to identify the sex of 2nd and 3rd-instar larvae and pupae. We selected the sex-chromosome male fertility gene *kl-5* (primer Kl5-F8 and Kl5-R6) as identifier for the males and used the autosomal *tpi* gene as a positive control (primer Tpi-F and Tpi-R) [49]. PCR amplifications were performed on the extracted DNA and a presence/absence gel-electrophoresis analysis was used to identify the sex of larvae.

Whole-body simultaneous RNA and DNA extraction for individual samples

M. pharaonis

For embryos and 1st-instar larvae, RNAs were extracted using PicoPure RNA Isolation Kits (Thermo Fisher), following the standard protocol, except embryos were first squashed with the blunt tip of a pulled glass capillary in order to homogenize and release the cell contents. For 2nd and 3rd-instar larvae, pre-pupae, pupae and callows, RNAs were extracted with RNeasy Plus Micro kits (Qiagen). During the lysis process, we used 5 mm stainless steel beads and added Reagent DX (Qiagen) and 2-Mercaptoethanol to the lysis buffer. DNAs were retrieved from 2nd and 3rd-instar larvae and pre-pupae by eluting the gDNA eliminator spin columns from the RNeasy Plus Micro kit. DNAs were recovered from the gDNA elimination column in the RNeasy Plus Micro kit by washing the column with AW1 and AW2 and eluting with AE buffer.

A. echinatior

RNAs and DNAs of 1st and 2nd-instar larvae in *A. echinatior* were extracted with RNeasy Plus Micro kits (Qiagen), following the same procedure as in *M. pharaonis*. For later stages, samples were sent to BGI sequencing service (Hong Kong) for whole body RNA extraction. Briefly, individuals were homogenized using a liquid nitrogen chilled mortar and pestle immediately following removal from the freezer. RNAs were extracted using TRIzol Reagent (Invitrogen) following a standard RNA-isolation protocol. For large individuals, a fraction of the homogenate was used so as not to exceed ~10% of TRI Reagent volume [50].

D. melanogaster

RNA of embryos and 1st-instar larvae were extracted with the PicoPure RNA Isolation Kit (ThermoFisher). RNA and DNA from all other stages were extracted using the RNeasy Plus Micro kit (Qiagen) following the same procedure as in *M. pharaonis*.

Testing RNA quality, constructing complementary DNA (cDNA) libraries and RNA sequencing

RNA quality testing, production of cDNA libraries, and sequencing were performed at BGI, China. The quality of RNA samples was tested with Agilent 2100 Bioanalyzer, and only samples with RIN > 4 were used for further analyses. Ambion ERCC RNA Spike-In Mix (catalogue number 4456740) was added to each sample according to the manufacturer's instructions before cDNA library construction, to be able to later verify the qualities of sequenced RNAseq data.

RNA sequences for each sample were first reverse transcribed into cDNA following the Smart-seq2 protocol [51], which was then randomly fragmented with Tn5 enzymes and linked with sequencing adapters to obtain a complete cDNA library for each individual sample. Primers were then added to the cDNA libraries for PCR amplification, and fragments ranging from 150 to 350 bp were selected for further cDNA circularization to construct sequencing libraries. The samples were then sequenced on a BGISEQ-500 platform using a 100nt paired-end sequencing protocol.

In-situ hybridization chain reaction

In situ probes

Sequences for LOC105837931 (*Freja*) (XM_012683128.3), *vasa* (XM_012686851.3), LOC105839887 (XM_036293539.1), LOC105830671 (*Smyd3*) (XM_036287663.1), actin5c (XM_012666578.3), tubulin (XM_012685189.3) and *septin2* (XM_012667189.2) were downloaded from NCBI and provided to Molecular Instruments for probe set synthesis. Alexa Fluor 488 was used for the detection of *vasa*; Alexa Fluor 546 was used for the detection of *Freja, actin5c* and *tubulin*; Alexa Fluor 594 was used for the detection of LOC105839887; and Alexa Fluor 647 was used for the detection of *Smyd3* and *septin2*.

RNA fluorescence *in situ* hybridization in *M. pharaonis* larvae and ovaries

RNA fluorescence *in situ* hybridization (FISH) was performed following the whole-mount drosophila HCR v3.0 protocol (Molecular Instruments; www.molecularinstruments.com/protocols) [17] with some modifications in that *M. pharaonis* larvae and ovaries were fixed at room temperature in scintillation vials with 50% FPE (4% formaldehyde; 0.5× PBS; 25 mM EGTA) and 50% heptane. Fixation time was then adjusted so that ovaries were fixed for 30 minutes, 1st and 2nd larval instars were fixed for 1-2 hours, and 3rd larval instars were fixed for 12 hours. Following fixation, the lower layer (FPE) was removed and replaced with methanol followed by vigorous shaking. The lower layer was replaced once more with methanol, at which point larvae and ovaries sink to the bottom of the vial. Larvae and ovaries were then dehydrated with several changes of methanol and stored at -20°C. Proteinase K concentration and treatment time was adjusted to 30 µg/mL for 7 minutes for 1st and 2nd larval instars and 10 minutes for 3rd larval instars and ovaries. Following amplification, one SSCT wash (5X SSC; 0.1% Tween-20; pH 7.0) was extended to 1 hour with the addition of 4',6-diamidino-2-phenylindole (DAPI; 1:1000) for nuclear staining in 1st and 2nd larval instars or overnight for 3rd larval instars and ovaries.

FISH-stained larvae and ovaries were then transferred into increasing concentrations of glycerol in 5xSSC and mounted in Vectashield or 70% glycerol/ 30% 5xSSC for imaging. Images were captured on a Leica SP5-X inverted confocal laser scanning microscope. Image stacks were processed using Fiji/ImageJ [52].

RNA interference experiments

Third instar reproductive (gyne or male) larvae were taken from nests and fixed with double-sided adhesive tapes. Interference double-strand RNA (dsRNA) was then injected into the upper ventral abdomen with a capillary needle (1B100F, World Precision Instrument), equipped on a micropipette puller (P-2000, Sutter) and Eppendorf FemtoJet injector (Femtojet 4i and Transferman 4r system, Eppendorf). For adult gynes, dsRNA was injected into the thorax, using the same equipment as in the larval injections, 5-, 7-, and 10-days after they had eclosed from the pupal stage. For both larval and adult RNAi, we used 7500 ng/ul of dsRNA in both experimental (*Freja*) and control (*GFP*) groups. To improve the efficiency in larval injection, lipofectamine 2000 (11668019, Thermo Fisher) was added in *Freja* and *GFP*

dsRNA liquid (dsRNA: lipofectamine 2000 = 3: 1). dsRNA was synthesized *in vitro*, following the instructions of the MEGAscript^{TM} RNAi Kit (AM1626, Thermo Fisher).

The *Freja* T7 primer sequences for dsRNA synthesis were:
Foreword: 5'-TAATACGACTCACTATAGGGCATCCATATCGTTGAAGGGC-3'.
Reverse: 5'-TAATACGACTCACTATAGGGGTCCAGGTCGGTGAAGTTGT-3'.
The *GFP* T7 primer sequences for dsRNA synthesis were:
Foreword: 5'-TAATACGACTCACTATAGGGAGTGCTTCAGCCGCTACCC-3'.
Reverse: 5'- TAATACGACTCACTATAGGGCATGCCGAGAGTGATCCCG-3'.

Quantification of tissue expression abundance with RT-qPCR
Heads, thoraxes and gasters (4th and higher abdominal segments) were dissected from newly eclosed gynes, and gasters were subdivided by tissue into digestive glands, cuticles, fat bodies and ovaries. Total mRNA of the dissected tissues was then isolated using TRIzol^{TM} reagent (15596018, Thermo Fisher). Reverse transcription was performed using the PrimeScriptTM RT reagent Kit with gDNA Eraser（RR047B, Takara, and mRNA levels were quantified using TB Green® Premix EX TaqTM II (Tli RNaseH Plus, RR820A, Takara) on a CFX96TM Real-Time system (BIO-RAD). Expression of *Freja* was normalized to the expression of *EF1α* in each sample.

The RT-qPCR primer sequences for *Freja* were:
Foreword: 5'- AACAGGGCAAACTCAGATATTTAC-3'.
Reverse: 5'- AGGCATCGATCGTTATCTCGG-3'.
The RT-qPCR primer sequences for *EF1α* were:
Foreword: 5'- TTCATTTATTGCTCTCACATCTACG -3'.
Reverse: 5'- ACCGTTGCCCTTTCTACTCTAA -3'.

Quantification of ovary developmental status
Ovary developmental status was quantified by the number and the surface area of yolky oocytes. Ovaries were dissected and collected from 12-day old gynes, where the number and the total surface area of yolky oocytes were counted and measured, respectively, from individual samples.

Juvenile hormone analog (JHA) and Precocene I feeding experiment
Third instar worker larvae of intermediate body length were treated with JH analog (JHA, Methoprene, MCE HY-B1161; 5mg/ml in 10% EtOH PBS solution), while control worker larvae were fed with 10% EtOH PBS solution. Both 0.5mg/ml JHA and 10% EtOH were mixed with foods and offered on day 1, 3 and 8. To confirm the efficiency of JHA, the treated worker larvae were collected 24 h after day 1 feeding. After isolating total RNA, the expression of *Kr-h1*, a downstream gene of juvenile hormone, was determined in both control and JHA groups. The expression of *Kr-h1* was normalized to *EF1a* in each sample. The RT-qPCR primer sequence for *Kr-h1* were:
Foreword: 5'- AGGATATAACGCAGCTTCCTGT -3'.
Reverse: 5'- GTGTGGCAGCGAACATTGTG -3'.

Third instar gyne larvae with intermediate body length were treated with 1% precocene I (sigma-195855; in 10% EtOH in PBS), while control gyne larvae were fed with 10% EtOH PBS solution. Both 1% precocene I and 10% EtOH were mixed with foods and offered on day 1, 3, 5 and 7.

To reveal the effects of JHA and precocene I on larval development, pupal stage samples were collected and body lengths measured under a stereomicroscope (SMZ18, Nikon). For JHA and control groups, cohort percentages of pupation on day 10, 15 and 20 were also recorded to check whether development time was affected. When pupae eclosed into adults, we measured their head width across the eyes and scape lengths (proxies of body size) in the control and JHA groups using the same stereomicroscope.

Transcriptome profiling and normalization

RNAseq data were first pre-processed with SOAPnuke (*version* 2.0.7) to remove adapters and to filter low quality reads [53]. Filtered RNAseq data were then mapped onto the transcriptome index of the corresponding species with *Salmon* (mapping-based mode) (*version* 1.4.0) [54], producing raw transcriptome abundance profiles (numbers of mapped reads for all annotated genes) for each of the individual samples.

The following genome assemblies and transcriptomic indexes were used for transcriptomic quantifications: *Monomorium pharaonis* (Chromosome level assembly GCF_013373865.1; NCBI annotation release 102), *Acromyrmex echinatior* (In-house assembly provided by Global Ant Genomics Alliance [55]; In-house annotation with GeMoMa (*version* 1.7.1) [56], using *Monomorium pharaonis*, *A. echinatior* [NCBI annotation release 100] and *Solenopsis invicta* [NCBI annotation release 103] as transcriptomic annotation reference), and *Drosophila melanogaster* (Genome assembly GCF_000001215.4; Flybase annotation release 6.32).

The raw transcriptome abundances (read counts or Transcripts Per Kilobase Million (TPM), used for cases of plotting gene expression levels) were log 2 transformed (after adding 1 to each score to avoid log 0) and then quantile normalized across samples to ensure that the overall distributions of gene expression levels remained the same across samples, which minimized the effects of any technical artefacts that might have occurred [57].

To ensure that results were robust to different normalization methods, we also applied variance stabilizing transformation (VST) [58] for each method before comparison. This procedure included three steps:(1) estimating the size factor (sequencing depth) of the raw transcriptome abundances for each of the samples; (2) estimating the dispersion-to-mean relationships across transcriptomes obtained from the raw transcriptome abundances after scaling by the size factor for each sample; and (3) normalising the transcriptome abundances for all samples using the fitted dispersion-to-mean relationships across transcriptomes. The resulting VST normalization thus takes both sequencing depth and dispersion-to-mean

relations into account, so the normalized transcriptome abundances become comparable across all samples and all genes with different expression levels [58].

We observed that these two normalization methods gave similar results, so we mainly used quantile normalization for the analyses except for the quantifications of within-stage transcriptome variation and between-caste variation, where we used VST to obtain a robust set of measurements.

Sample quality control

Besides removing samples with low RNA quality (RIN < 4), we also discarded samples with poor RNAseq quality, either due to technical biases, e.g. cDNA library construction or sequencing, or when being biological outliers, e.g. delayed growth or dead samples. Within each species, we first calculated the transcriptome (normalized gene expression profile) similarities between any two samples and then measured by their pairwise Spearman's correlation coefficients. In the comparisons that followed for each developmental stage, samples were then considered to be outliers if their within-stage transcriptome similarity was low (Spearman's correlation coefficient < 0.8) [59].

Correction for batch effects

Although RNA extraction, cDNA library construction and sequencing were all done with similar procedures (except for embryos and 1st instar samples for which we used a different extraction kit), we noticed a systematic expression difference for samples that had been sequenced before July 2018 (Batch A; 925 samples), before April 2019 (Batch B; 329 samples) and afterwards (Batch C;169 samples), producing three technical batches that could potentially confound the comparative analyses, especially among samples in *A. echinatior*. However, we found that removing batch B and C did not significantly impact our conclusions and therefore retained all samples to attain a maximally complete coverage of all developmental stages.

To correct for the batch effects, we used the body length measurements and the even distribution of batches across developmental stages. We estimated the batch effects on the gene expression level with the following linear regression model:

$$Exp_{gene} \sim batch_{gene} + age * (caste + log(bodylength))$$

We assumed that the batch effects on each gene's expression level were consistent between castes and across developmental stages and that the effect of body length on gene expression level was consistent between castes within the same developmental stage. We then used a linear regression model to estimate putative batch effects. After partialing out the variance component that could have been due to batch effect, we obtained gene expression levels of same-caste and same-stage individuals that were similar across batches, and an expected overall transcriptomic expression pattern where individuals of the same caste and same developmental stage clustered together regardless of batch. We then used these adjusted gene expression levels for all downstream analyses, except for transcriptome variation analyses. Differences in expression variation cannot be corrected by regression-based batch corrections, so we excluded samples of the minority batch for these analyses.

Constructing the developmental trajectory network

Within each species, the developmental trajectory network was constructed based on the transcriptomic similarities among all samples. These similarities, as described in *Sample quality control*, formed a pair-wise similarity matrix among all samples. We used the values of this matrix to construct a weighted un-directed network, where nodes represent samples and edges represent similar transcriptome profiles between connected samples. The weights of edges were measured by the Spearman's correlation coefficient among samples, indicating the level of transcriptome similarity. To increase the overall signal of the network, we removed weak connecting edges (weight < 0.8), a threshold criterion based on the empirical suggestion that correlation coefficients for anisogenic samples should be higher than 0.8 [59].

The weighted un-directed network was then visualized with the force-directed layout algorithm using the *igraph* package (*version* 1.2.9) in R [60]. This algorithm takes the weights of edges into account, so that nodes with strong edges, i.e. samples with high transcriptome abundance similarities, are clustering together. For visualization purposes, we set edges' colour according to edges' weight, ranging from white (weight = 0.8) to black (weight = 1).

Detection of orthologs and homologs across species

Orthologs among *M. pharaonis*, *A. echinatior* and *D. melanogaster* were identified with Orthofinder (*version* 2.5.4), a phylogeny-based ortholog inference method [61]. To infer orthologs, we used the proteomes of 17 species (16 from NCBI and one, *A. echinatior,* from our in-house annotated proteome as its PacBio genome annotation is not yet available in NCBI). These included 11 species of Hymenoptera, including four ant species (*A. echinatior*, *M. pharaonis*, *Ooceraea biroi* and *Harpegnathos saltator*), three bee species (*Apis mellifera*, *Bombus terrestris* and *Osmia lignaria*), three wasps species (*Polistes dominula*, *Vespa mandarinia* and *Nasonia vitripennis*) and the sawfly *Cephus cinctus*. We also included six non-hymenopteran species, i.e. two fly species (*D. melanogaster* and *D. willistoni*), one mosquito (*Aedes albopictus*), one moth (*Bombyx mori*), one beetle (*Photinus pyralis*) and one butterfly (*Maniola hyperantus*). For genes with multiple isoforms, we always used the longest protein as the representative sequence.

We then used the default parameters in OrthoFinder to detect orthologs, except when using BLAST (ver. 2.12.0) [62] for similar sequence searching and multiple sequence alignment for gene tree inference, which provided the best ortholog inference performance according to the benchmark test [61]. For genes with multiple orthologs, the most similar ortholog was used but information for all orthologs is provided in the Supplementary materials. Orthologs were used for downstream comparative transcriptomic analyses, functional enrichment analyses, and tissue-specific relative expression abundance estimation.

Alignment of developmental transcriptomes and measurement of between-species transcriptomic similarity

Rate of development and number of instars differ between ant species and castes [1,63]. In our study species, there are three larval instars in *M. pharaonis* and three to four in *A. echinatior*.

Embryogenesis in *M. pharaonis* lasts for ca. 9 days, which is long compared to *D. melanogaster* where eggs hatch after ca. 24 hours. Developmental stages thus need to be aligned between species before comparative analyses can be done.

To align developmental stages, either between castes or between species, we measured developmental stage similarities by their overall transcriptomic distance, calculated as 1 – Spearman's correlation coefficient of transcriptomes (or orthologous transcriptomes for cross species comparison). Stages with the lowest overall transcriptomic distance (mean value for all same stage samples) were assessed as the best matched (aligned) stages and used for downstream between-caste and between-species comparisons.

Between-species transcriptomic similarity for each developmental stage was calculated as the mean value of 1 - Spearman's correlation coefficients among samples of the best aligned stages, separately for each caste.

The Backward Progressives Algorithm (BPA)

We developed a new algorithm that allows backwards prediction of caste identity based on the sequential overall transcriptomic patterns. The algorithm compares (1) the transcriptomes of individuals at a target developmental stage with unknown caste identity, and (2) the transcriptomes of individuals at the later stage where caste identity was known or had been assigned in a previous round. For each round of prediction, BPA performed four steps: normalization, feature selection, model training, and prediction.

Because prediction data (of differentiation in unassigned transcriptomes of the target developmental stage) and training data (caste-assigned transcriptomes from the subsequent stage) represent two continuous developmental stages next to each other in time, developmental effects are expected to always contribute, but with quantitatively different effects, to both data sets. The first step of BPA (Normalization) therefore removes such developmental effects by subtracting the mean expression levels and normalizing the expression variation across the two data sets, using the Combat package (from *sva* (*version* 3.40.0)) in R, which sets developmental stage as batch co-variate [64]. The normalized transcriptomes thus represent expression levels that are independent of developmental stage and with a maximal likelihood to reflect segregation by caste in both data sets.

The second essential step of BPA is feature selection. This starts with a Principal Component Analysis (PCA) of the prediction data, assuming that one or several of the PC axes from this data set should be related to as yet unspecified caste identities in the target stage. We thus assumed that one or several of the top PC axes should include the best possible set of caste PC axes driven by the expression difference between the caste phenotypes not yet identified. The second sub-step of feature selection is then to confront these PC axes with training data, by projecting them on the samples of the subsequent developmental stage. This comparison uses singular value decomposition (SVD) to extract the coefficients of each PC axis and then multiplies them with the training data. This process produces new PC scores for each individual in the training data, which then allows the third sub-step of identifying the PC axes

that best separate the known caste identities in the training data when performing ANOVA. The most significant PC axes are then assumed to be the shared caste PCs for both prediction and training data.

With the selected candidate feature (the best fitting PC axes for caste) in place, the third and fourth steps of BPA are model training and prediction. We first applied linear discriminant analysis on the known caste PC values to train a predictive model for caste segregation. We then predicted individual caste identities of target stage individuals and assigned a probability of being gyne (reproductive of unspecified sex before the 2nd larval instar) or worker to each individual. Once a complete round is completed, a prediction result for developmental stage n (S_n) can then be used to predict individual caste identities of transcriptomes at stage n -1 (S_{n-1}), following the same four steps as in the previous round of prediction, except that now the samples at S_{n-1} were used as prediction data and the samples at S_n as training data.

For BPA prediction of 1st instar larvae in *M. pharaonis*, we used the body size independent caste DEGs of 2nd instar larvae (number of genes = 173) for feature selection. Body size independent caste DEGs were identified from samples of these 2nd instar larvae with approximately equal body lengths (ranging between 0.52 and 1.08 mm), using DESeq2 [58] with the model: $Exp \sim caste + log(body\ length)$ (see *Detecting differentially expressed genes between castes*). A gene was retained for feature selection if its adjusted *P* value was < 0.05 and its log2 expression fold change between castes was > 0.5. Compared to using all genes, our use of caste DEGs for feature selection significantly increased the accuracy in our testing data set (see *Testing the accuracy of BPA*; Extended Data Fig. 2c), probably because it removed the housekeeping genes whose expression is unrelated to caste differentiation.

Testing the accuracy of BPA

We tested *BPA* on data sets of five later developmental stages for which caste identity was known and found that accuracies of single stage prediction were 86-100% (Extended Data Fig. 2c). *M. pharaonis* individuals beyond the pre-pupal stage could all be correctly assigned to their observed caste identities, but we observed a gradual decline in BPA accuracy when we conducted backward caste reconstructions for earlier stages. For example, BPA-accuracy dropped to 73% when working backwards from 2nd instar larvae. This is as expected because prediction errors increase multiplicatively across sequential rounds and because transcriptomic differences between castes are likely to be less pronounced in earlier developmental stages. We therefore only used BPA predictions in larval stages where experimental validation was possible.

Testing the influence of sex on early developmental transcriptomes in *M. pharaonis*

The small biomass of 1st instar larvae (and of the earlier embryos) precluded extracting DNA for microsatellite genotyping to remove haploid male individuals. However, we found that validated 2nd instar larval transcriptomes for gynes and males were very similar when compared to significantly different 2nd instar worker larvae (Extended Data Fig. 2f), indicating that early transcriptomic differentiation primarily reflects differences between reproductive (gynes and males) and sterile (worker) developmental trajectories.

Quantification of transcriptome variation and difference

Within-stage transcriptome variation was measured by the mean value of 1 – Spearman's correlation coefficients between the transcriptomes of target samples and the transcriptomes of all other samples within the same stage, regardless caste identities for overall measurement, or separately for each caste for within-caste measurement.

Between-caste transcriptomic differences were calculated as the average expression difference between gynes and workers (of the same stage) for all genes. The expression difference of a single gene was calculated as:

$$\mathrm{Dif}_{\mathrm{gene}} = \left|\overline{Exp_{gyne}} - \overline{Exp_{worker}}\right|$$

where the absolute value serves to remove the likelihood sign difference for worker or gyne bias.

As the gene expression levels were already normalized by log2, the expression difference between castes is equivalent to the absolute value of log2 expression fold change between castes.

Quantification of caste developmental potential.

Developmental potential of target individuals was based on the transcriptomic distance between a target individual and its focal caste (measured as the average transcriptome of all same-caste individuals) at the subsequent developmental stage. If the transcriptomic distance between a target individual and a representative gyne was smaller than the distance between that target individual and a representative worker, the target individual was classified as being more likely to start developing into (or continue its development into) a gyne rather than a worker.

We first normalized the mean transcriptomic difference between stages by standardizing the expression level of each gene for all same-stage individuals. This step removed the quantitative differences between developmental stages (see first step, Normalization in the BPA description). We then calculated the developmental potential (Δ) of each individual (*i*) with the following formula:

$$\Delta_{\mathrm{X,t}} = \frac{\mathrm{dist(i, worker_{t+1})} - \mathrm{dist(i, gyne_{t+1})}}{\mathrm{dist(gyne_{t+1}, worker_{t+1})}}$$

Here, $dist(i, caste_{t+1})$ is the transcriptomic distance between individual *i* and the focal caste at the subsequent stage and is calculated as the Manhattan distance, a robust measure for transcriptomes that is commonly used for arithmetic calculations. The transcriptomic distance difference between castes was then normalized by $dist(gyne_{t+1}, worker_{t+1})$, which measures the transcriptomic distance between a focal gyne and a focal worker at the subsequence stage, so that $\Delta_{X,t}$ becomes a dimensionless measure. $\Delta_{X,t}$ = 1 then indicates that

individual *i* is equivalent to a representative gyne in the subsequent stage while $\Delta_{X,t}$ = -1 indicates that the individual is equivalent to the representative worker.

Quantification of gene-level canalization scores

Gene level canalization scores were calculated based on the developmental dynamics of expression divergence between gyne and worker castes. For each developmental stage with known/predicted caste phenotypes, we first calculated a modified *t* score for expression divergence of a target gene (*g*) as:

$$t_g = \frac{\overline{Exp}_{gyne} - \overline{Exp}_{worker}}{s_p}$$

Here, s_p is the pooled standard deviation for the expression levels of gynes and workers:

$$s_p = \sqrt{S_{gyne}^2 + S_{worker}^2}$$

A high absolute value of a *t* score indicates a high between-caste expression difference or a low within-caste expression variance(s).

Based on the *t* scores across developmental stages, we then quantified the canalization score (*C*), to measure the developmental trend for the expression differences between castes. We defined the canalization score as:

$$C_g = -\log_{10}(P_g) \ * \ t_{g,\,final}$$

where P_g is the *P* value of the correlation test for the absolute values of *t* scores across developmental stages and $t_{g,final}$ is the *t* score of the late pupal stage when the morphological differentiation process between gynes and workers is largely completed. With the canalization score, we can thus capture the canalization level for each gene, because a high value of $-log_{10}(P_g)$ indicates an increasing between-caste difference or a decreasing within-caste variance across developmental stages, and a high absolute value of $t_{g,final}$ indicates a large between-caste expression divergence at the terminal stage.

Based on these canalization scores, we defined a gene as being canalized if P_g was < 0.05 and the absolute value of C_g was higher than 3.

Identifying the <u>phylogenetic</u> origin of *Freja*

To identify the phylogenetic origin of *Freja* (NCBI ID: LOC105837931), we identified the ortholog group of this gene, i.e., the set of genes (including both orthologs and paralogs) descended from a single gene in the last common ancestor. The ortholog group was identified (with Orthofinder) among the 17 selected species, including 11 Hymenoptera and 6 species outside the Hymenoptera (see *Detection of orthologs and homologs across species*). All gene members of the *Freja* ortholog group were found in the Hymenoptera, indicating that *Freja* is a hymenopteran order-specific gene.

We then performed multiple sequence alignments on the protein sequences of the ortholog group, using T-coffee (*version* 13.45.0) with default parameters [65]. With the aligned protein

sequences, we reconstructed a gene tree, using IQ-TREE (*version* 2.1.4) with 1000 replicates for bootstrapping and 1000 replicates for SH approximate likelihood ratio test [66].

Body-length threshold regression model

To identify the threshold for a change in expression dynamics at a certain larval body size, gene expression levels of each caste were fitted with a continuous two-phase (segmented) model (M11) using the R package *chngpt* (*version* 2021.5-12) [28]. The threshold model can be expressed as:

$$Exp \sim \alpha * body\ size_{before} + \beta * body\ size_{after}$$

Here, the threshold regression model detects a significant change of slopes (α and β) before and after a body size threshold, and a threshold model is significant if the *P* value for the log likelihood ratio test between the threshold model and the null model, *Exp ~ body size*, is < 0.05.

Detecting differentially expressed genes (DEGs) between castes

Caste differentially expressed genes (DEGs) at each developmental stage were detected using the DESeq2 (*version* 1.32.0) package in R [58]. For all samples within each developmental stage, a read count matrix of transcriptomes (output from the Salmon mapping; see above) was loaded using tximport [67], which integrated expression profiles from the transcript-level to the gene-level. With these gene-level transcriptomes, we then used DESeq2 to model the expression level of each gene as: $Exp \sim caste$, and we defined genes as caste DEGs for a target developmental stage if their adjusted *P* values were < 0.05.

To reduce the confounding effect of body size on gene expression difference between castes (e.g., 2nd instar sexuals are always larger than 2nd instar workers, so the expression difference might be the result of a larger body size) [20], we further integrated body length measurement to adjust slopes for the influence of body length and thus identify body size independent caste DEGs for 2nd instar larvae. The expression level of each gene was modelled as:

$$Exp \sim caste + log(body\ length)$$

A gene was then assessed as a body size independent caste DEG if the adjusted *P* value for caste was less than 0.05 and there was at least a 1.6-fold expression difference between castes. The expression difference between castes was estimated with a robust linear regression model [68].

Functional enrichment and loss of function enrichment analyses.

Functional enrichment and loss of function enrichment analyses for target gene sets in ants were done based on their homologs in *D. melanogaster*. Protein sequences of *M. pharaonis* and *A. echinatior* were first annotated with their *Drosophila* homologs' Gene Ontology (GO), Kyoto Encyclopedia of Genes and Genomes (KEGG) information and allele loss of function phenotypes from Flybase [69]. Functional enrichments were then obtained by over-representation tests with the clusterProfiler package (*version* 4.0.5) [70], evaluating the percentage of genes in particular functional categories (e.g. biological functions or pathways) among the target gene set, e.g. caste DEGs. Functional categories were accepted as significantly over-represented (enriched) if their *P* values < 0.05 and *q* values < 0.1.

The enriched functional terms contained redundant terms with similar gene members and functions. To provide a concise description of gene functions, we therefore further clustered the enriched terms based on their gene membership similarities, calculated by the ratio of the number of shared gene members and the number of total non-redundant gene members. These similarities range between 0 to 1, with 1 indicating a complete overlap of gene members. For each term cluster, we then used the most significant term, ranked by their *P* values in the enrichment analysis, as the representative term. A full list of enriched functional terms is provided in Supplementary table 5.

Determination of tissue origins of gene expression based on *Drosophila* database

Tissue origin of expression of target genes were based on the *Drosophila melanogaster* gene expression atlas (FlyAtlas2) [29]. For larval stages, we used the expression data from larval main tissues, including brain, midgut, hindgut, malpighian tubules, fat body, salivary gland and trachaea, and calculated the relative expression level based on their TPM values:

$$\mathrm{REx}p_{tissue} = \frac{log_2(TPM_{tissue}+1)}{\sum(log_2(TPM_{tissue}+1))},$$

where one pseudo count was added to obtain a robust estimation in case of low TPM values.

For the pupal and adult stages, we used the expression data from adult female tissues, including brain, eye, thoracicoabdominal ganglion, midgut, hindgut, Malpighian tubules, fat body, salivary gland and ovary. Relative expression levels were calculated as in the larval stages (see above).

References:

1. Wheeler, W. M. *Ants; their structure, development and behavior, by William Morton Wheeler ...* (Columbia University Press, 1910). doi:10.5962/bhl.title.1937.

2. Boomsma, J. J. & Gawne, R. Superorganismality and caste differentiation as points of no return: how the major evolutionary transitions were lost in translation. *Biol Rev* 93, 28–54 (2017).

3. Waddington, C. H. *The Strategy of the Genes: A Discussion of Some Aspects of Theoretical Biology*. (Allen & Unwin, 1957).

4. Waddington, C. H. *Organisers and Genes*. (The University Press, 1940).

5. Farrell, J. A. *et al.* Single-cell reconstruction of developmental trajectories during zebrafish embryogenesis. *Science* 360, eaar3131 (2018).

6. Wagner, D. E. *et al.* Single-cell mapping of gene expression landscapes and lineage in the zebrafish embryo. *Science* 360, eaar4362 (2018).

7. Sladitschek, H. L. *et al.* MorphoSeq: Full Single-Cell Transcriptome Dynamics Up to Gastrulation in a Chordate. *Cell* 181, 922-935.e21 (2020).

8. Schiebinger, G. *et al.* Optimal-Transport Analysis of Single-Cell Gene Expression Identifies Developmental Trajectories in Reprogramming. *Cell* 176, 928--943 (2019).

9. Schrader, L., Simola, D. F., Heinze, J. & Oettler, J. Sphingolipids, Transcription Factors, and Conserved Toolkit Genes: Developmental Plasticity in the Ant Cardiocondyla obscurior. *Molecular Biology and Evolution* 32, 1474–1486 (2015).

10. Warner, M. R., Qiu, L., Holmes, M. J., Mikheyev, A. S. & Linksvayer, T. A. Convergent eusocial evolution is based on a shared reproductive groundplan plus lineage-specific plastic genes. *Nat Commun* 10, 2651 (2019).

11. Warner, M. R., Mikheyev, A., er S & Linksvayer, T. A. Genomic Signature of Kin Selection in an Ant with Obligately Sterile Workers. *Mol Biol Evol* 34, 1780--1787 (2016).

12. Adams, R. M. M. *et al.* Hairs distinguish castes and sexes: Identifying the early ontogenetic building blocks of a fungus-farming superorganism (Hymenoptera: Formicidae). *Myrmecological News.* 31, 201–216 (2021).

13. Schmidt, A. M., D'Ettorre, P. & Pedersen, J. S. Low levels of nestmate discrimination despite high genetic differentiation in the invasive pharaoh ant. *Front Zool* 7, (2010).

14. Qiu, B. *et al.* Towards reconstructing the ancestral brain gene-network regulating caste differentiation in ants. *Nat Ecol Evol* 2, 1782–1791 (2018).

15. Pontieri, L. *et al.* From egg to adult: a developmental table of the ant Monomorium pharaonis. *Biorxiv* 2020.12.22.423970 (2020) doi:10.1101/2020.12.22.423970.

16. Holmberg, J. & Perlmann, T. Maintaining differentiated cellular identity. *Nature Reviews Genetics* 13, 429–439 (2012).

17. Choi, H. M. T. *et al.* Third-generation in situ hybridization chain reaction: multiplexed, quantitative, sensitive, versatile, robust. *Development* 145, dev165753 (2018).

18. Khila, A. & Abouheif, E. Reproductive constraint is a developmental mechanism that maintains social harmony in advanced ant societies. *Proc National Acad Sci* 105, 17884–17889 (2008).

19. Truman, J. W. & Riddiford, L. M. The evolution of insect metamorphosis: a developmental and endocrine view. *Philosophical Transactions Royal Soc B Biological Sci* 374, 20190070 (2019).

20. Montgomery, S. H. & Mank, J. E. Inferring regulatory change from gene expression: the confounding effects of tissue scaling. *Mol Ecol* 25, 5114–5128 (2016).

21. Nijhout, H. F. *et al.* The developmental control of size in insects. *Wiley Interdiscip Rev Dev Biology* 3, 113–134 (2014).

22. Zhou, X., Tarver, M. R. & Scharf, M. E. Hexamerin-based regulation of juvenile hormone-dependent gene expression underlies phenotypic plasticity in a social insect. *Development* 134, 601–610 (2006).

23. Libbrecht, R. *et al.* Interplay between insulin signaling, juvenile hormone, and vitellogenin regulates maternal effects on polyphenism in ants. *Proc National Acad Sci* 110, 11050–11055 (2013).

24. Penick, C. A., Prager, S. S. & Liebig, J. Juvenile hormone induces queen development in late-stage larvae of the ant Harpegnathos saltator. *Journal of insect physiology* 58, 1643–1649 (2012).

25. Shinoda, T. & Itoyama, K. Juvenile hormone acid methyltransferase: A key regulatory enzyme for insect metamorphosis. *Proc National Acad Sci* 100, 11986–11991 (2003).

26. Belles, X. Krüppel homolog 1 and E93: The doorkeeper and the key to insect metamorphosis. *Arch Insect Biochem* 103, e21609 (2020).

27. Amsalem, E., Teal, P., Grozinger, C. M. & Hefetz, A. Precocene-I inhibits juvenile hormone biosynthesis, ovarian activation, aggression and alters sterility signal production in bumble bee (Bombus terrestris) workers. *J Exp Biol* 217, 3178–3185 (2014).

28. Fong, Y., Huang, Y., Gilbert, P. B. & Permar, S. R. chngpt: threshold regression model estimation and inference. *Bmc Bioinformatics* 18, 454 (2017).

29. Leader, D. P., Krause, S. A., Pandit, A., Davies, S. A. & Dow, J. A. T. FlyAtlas 2: a new version of the Drosophila melanogaster expression atlas with RNA-Seq, miRNA-Seq and sex-specific data. *Nucleic Acids Res* 46, gkx976- (2017).

30. Wu, X., Tanwar, P. S. & Raftery, L. A. Drosophila follicle cells: Morphogenesis in an eggshell. *Semin Cell Dev Biol* 19, 271–282 (2008).

31. Dijkstra, M. B., Zweden, J. S. van, Dirchsen, M. & Boomsma, J. J. Workers of Acromyrmex echinatior leafcutter ants police worker-laid eggs, but not reproductive workers. *Anim Behav* 80, 487–495 (2010).

32. Wheeler, W. M. The ant-colony as an organism. *J Morphol* 22, 307--325 (1911).

33. Extavour, C. G. & Akam, M. Mechanisms of germ cell specification across the metazoans: epigenesis and preformation. *Development* 130, 5869–5884 (2003).

34. Corona, M., Libbrecht, R. & Wheeler, D. E. Molecular mechanisms of phenotypic plasticity in social insects. *Curr Opin Insect Sci* 13, 55–60 (2015).

35. Korb, J. & Belles, X. Juvenile hormone and hemimetabolan eusociality: a comparison of cockroaches with termites. *Curr Opin Insect Sci* 22, 109–116 (2017).

36. Barchuk, A. R. *et al.* Molecular determinants of caste differentiation in the highly eusocial honeybee Apis mellifera. *BMC Developmental Biology* 7, 70 (2007).

37. Nijhout, H. F. & Wheeler, D. E. Juvenile Hormone and the Physiological Basis of Insect Polymorphisms. *Q Rev Biology* 57, 109–133 (1982).

38. Trible, W. & Kronauer, D. J. C. Ant caste evo-devo: size predicts caste (almost) perfectly. *Trends Ecol Evol* 36, 671–673 (2021).

39. Briggs, J. A. *et al.* The dynamics of gene expression in vertebrate embryogenesis at single-cell resolution. *Science* 360, (2018).

40. Cao, J. *et al.* The single-cell transcriptional landscape of mammalian organogenesis. *Nature* 566, 496–502 (2019).

41. Edwards, J. P. *Caste regulation and determination in the pharaoh's ant Monomorium pharaonis (L.)*. (1984).

42. Khila, A. & Abouheif, E. Evaluating the role of reproductive constraints in ant social evolution. *Philosophical Transactions Royal Soc B Biological Sci* 365, 617–630 (2010).

43. Schwander, T., Lo, N., Beekman, M., Oldroyd, B. P. & Keller, L. Nature versus nurture in social insect caste differentiation. *Trends Ecol Evol* 25, 275–282 (2010).

44. Jiang, L. *et al.* Synthetic spike-in standards for RNA-seq experiments. *Genome Res* 21, 1543--1551 (2011).

45. Edwards, J. P. Caste regulation in the pharaoh's ant Monomorium pharaonis: recognition and cannibalism of sexual brood by workers. *Physiol Entomol* 16, 263–271 (1991).

46. Boonen, S. & Billen, J. Caste regulation in the ant Monomorium pharaonis (L.) with emphasis on the role of queens. *Insect Soc* 64, 113–121 (2017).

47. Peacock, A. D., Haul, D. W., Smith, I. C. & Goodfellow, A. The Biology and Control of the Ant Fest Monomorium pharaonis (L.). *The Biology and Control of the Ant Fest Monomorium pharaonis (L.).* (1950).

48. Dijkstra, M. B. & Boomsma, J. J. The economy of worker reproduction in Acromyrmex leafcutter ants. *Anim Behav* 74, 519–529 (2007).

49. Dyer, K. A., White, B. E., Bray, M. J., Piqué, D. G. & Betancourt, A. J. Molecular Evolution of a Y Chromosome to Autosome Gene Duplication in Drosophila. *Mol Biol Evol* 28, 1293–1306 (2011).

50. Hunt, B. G. & Goodisman, M. A. D. Evolutionary variation in gene expression is associated with dimorphism in eusocial vespid wasps. *Insect Mol Biol* 19, 641–652 (2010).

51. Picelli, S. *et al.* Full-length RNA-seq from single cells using Smart-seq2. *Nat Protoc* 9, 171 (2014).

52. Schindelin, J. *et al.* Fiji: an open-source platform for biological-image analysis. *Nat Methods* 9, 676–682 (2012).

53. Chen, Y. *et al.* SOAPnuke: a MapReduce acceleration-supported software for integrated quality control and preprocessing of high-throughput sequencing data. *Gigascience* 7, 1--6 (2018).

54. Patro, R., Duggal, G., Love, M. I., Irizarry, R. A. & Kingsford, C. Salmon provides fast and bias-aware quantification of transcript expression. *Nat Methods* 14, 417--419 (2017).

55. Boomsma, J. J. *et al.* The Global Ant Genomics Alliance (GAGA). *Myrmecological News* 25, 61–66 (2017).

56. Keilwagen, J. *et al.* Using intron position conservation for homology-based gene prediction. *Nucleic Acids Research* 44, e89–e89 (2016).

57. Zyprych-Walczak, J. *et al.* The Impact of Normalization Methods on RNA-Seq Data Analysis. *Biomed Res Int* 2015, (2015).

58. Love, M. I., Huber, W. & Anders, S. Moderated estimation of fold change and dispersion for RNA-seq data with DESeq2. *Genome Biol* 15, (2014).

59. Encode-Consortium. ENCODE Guidelines and Best Practices for RNA-Seq. https://www.encodeproject.org/documents/cede0cbe-d324-4ce7-ace4-f0c3eddf5972/@@download/attachment/ENCODE%20Best%20Practices%20for%20RNA_v2.pdf (2016).

60. Csardi, G. & Nepusz, T. The igraph software package for complex network research. *InterJournal* Complex Systems, 1695 (2006).

61. Emms, D. M. & Kelly, S. OrthoFinder: phylogenetic orthology inference for comparative genomics. *Genome Biol* 20, 238 (2019).

62. Altschul, S. F., Gish, W., Miller, W., Myers, E. W. & Lipman, D. J. Basic local alignment search tool. *J Mol Biol* 215, 403–410 (1990).

63. Schultner, E., Oettler, J. & Helanterä, H. The Role of Brood in Eusocial Hymenoptera. *Q Rev Biology* 92, 39–78 (2017).

64. Leek, J. T., Johnson, W. E., Parker, H. S., Jaffe, A. E. & Storey, J. D. The SVA package for removing batch effects and other unwanted variation in high-throughput experiments. *Bioinformatics* 28, 882--883 (2012).

65. Notredame, C., Higgins, D. G. & Heringa, J. T-coffee: a novel method for fast and accurate multiple sequence alignment11Edited by J. Thornton. *J Mol Biol* 302, 205–217 (2000).

66. Minh, B. Q. *et al.* IQ-TREE 2: New models and efficient methods for phylogenetic inference in the genomic era. *Mol Biol Evol* 37, 1530–1534 (2020).

67. Soneson, C., Love, M. I. & Robinson, M. D. Differential analyses for RNA-seq: transcript-level estimates improve gene-level inferences. *F1000research* 4, 1521 (2016).

68. Huber, P. J. *Robust Statistics*. (1981). doi:10.1002/0471725250.ch1.

69. Larkin, A. *et al.* FlyBase: updates to the Drosophila melanogaster knowledge base. *Nucleic Acids Res* 49, D899–D907 (2020).

70. Wu, T. *et al.* clusterProfiler 4.0: A universal enrichment tool for interpreting omics data. *Innovation* 2, 100141 (2021).

Acknowledgments:

We thank the China National Genebank for providing transcriptomics sequencing service with MGI sequencers. This work was supported by the Lundbeck Foundation (grant no. R190-2014-2827 to G.Z.), the Villum Foundation (Villum Investigator Grant, grant no. 25900 to G.Z.), the European Research Council (Advanced Grant no. 323085 to J.J.B.), the National Natural Science Foundation of China (grant no. 31820573 to G.Z.; no. 31501057 to Q.L., and no. 31900399 to W.L.).

Author contributions:

B.Q., J.J.B. and G.Z. conceived the project. B.Q., X.D., R.S.L., W.L. and G.Z. designed the experiments. B.Q. and G.Z. developed the bioinformatic methods. B.Q. analysed the data. X.D., P.L., R.S.L. and R.L. led experimental work, assisted by B.Q., A.L.P., G.D., M.J.T., X.Z., D.Z., Q.G., T.W., L.P. and L.W. B.Q. and P.L. managed the data, assisted by R.S.L., W.J. and C.G. K.R., Q.L., W.L. and G.Z. provided resources for the experiments. B.Q., J.J.B. and G.Z. prepared the manuscript, assisted by X.D., R.S.L., R.L., A.L.P. and M.J.T.

Competing interests:

The authors declare no competing interests.

Materials & Correspondence:

B.Q. and G.Z. are responsible for the transcriptomic data, which are archived at NCBI GEO (BioProject Number PRJNA767561).
B.Q. is responsible for the computational codes used in this paper. Main codes can be found at: https://github.com/BitaoQiu/devo-ants

Supplementary Files

This is a list of supplementary files associated with this preprint. Click to download.

- NEEExtendedDatafinal.docx
- SupplementaryTable1PredictedcasteDEGsfor1stinstarlarvae.xlsx
- SupplementaryTable2ListofcasteDEGsateachdevelopmentalstage.xlsx
- SupplementaryTable3FunctionalenrichmentforcasteDEGsateachdevelopmentalstage.xlsx
- SupplementaryTable4Tableofcanalizedgenes.xlsx
- SupplementaryTable5Functionalenrichmentofcanalizedgenes.xlsx